LETTERS
https://doi.org/10.1038/s41566-021-00830-x

nature photonics

High-temperature superfluorescence in methyl ammonium lead iodide

Gamze Findik[1,3], Melike Biliroglu[1,3], Dovletgeldi Seyitliyev[1], Juliana Mendes[2], Andrew Barrette[1], Hossein Ardekani[1], Lei Lei[2], Qi Dong[2], Franky So[2] and Kenan Gundogdu[1]✉

Light–matter interactions can create and manipulate collective many-body phases in solids[1–3], which are promising for the realization of emerging quantum applications. However, in most cases, these collective quantum states are fragile, with a short decoherence and dephasing time, limiting their existence to precision tailored structures under delicate conditions such as cryogenic temperatures and/or high magnetic fields. In this work, we discovered that the archetypal hybrid perovskite, $MAPbI_3$ thin film, exhibits such a collective coherent quantum many-body phase, namely superfluorescence, at 78 K and above. Pulsed laser excitation first creates a population of high-energy electron–hole pairs, which quickly relax to lower energy domains and then develop a macroscopic quantum coherence through spontaneous synchronization. The excitation fluence dependence of the spectroscopic features and the population kinetics in such films unambiguously confirm all the well-known characteristics of superfluorescence. These results show that the creation and manipulation of collective coherent states in hybrid perovskites can be used as the basic building blocks for quantum applications[4,5].

Spontaneous synchronization of oscillators is a fascinating process. Although it is best visualized as the buildup of a collective phase in initially randomly oscillating metronomes coupled to the same medium, spontaneous synchronization is a universal phenomenon occurring in natural processes such as the initial ordering of planetary orbits, frequency locking of triode generators and signal synchronization of fireflies[6]. This phenomenon prevails in both macro and micro realms, spanning physical and biological systems, and leads to the manifestation of exotic collective quantum phenomena[3]. In the quantum domain, systems are described by wavefunctions in which the 'phase' plays a dominant role determining the waveform and its relation to other waves, along with their collective behaviour under external stimuli. Although an incoherent population of quantum objects has a random distribution of phases, spontaneous synchronization leads to symmetry breaking and the observation of exotic collective quantum phenomena, including, but not limited to, superconductivity, Bose–Einstein condensation and the collective dynamics of Josephson junctions[7].

A remarkable example of spontaneous synchronization is the superfluorescence of optically excited dipoles in a small volume. Figure 1 illustrates the process. Here, an initially excited dipole population has a random phase distribution. The vacuum field interactions spontaneously synchronize the phases of these oscillators and the system transitions into the Dicke superradiant state[8–10]. In this coherent state, all the excitations act like a giant atom and interact with the radiation field collectively, emitting a high-intensity short burst of photons. This phase transition of an ensemble of incoherent dipoles into a coherent macroscopic quantum state and its collective radiation is called superfluorescence (SF).

The superfluorescent phase transition depends on the coherence time. SF can only form if the dephasing is slower than spontaneous synchronization. Accordingly, SF has been primarily observed in gas-phase systems[11–13]. Fast electronic dephasing in condensed matter limits the observation of SF to a handful of solids at cryogenic temperatures. These include oxygen-doped KCl[14], CuCl nanocrystals embedded into a NaCl matrix[15], bulk ZnTe single crystals[16] and InGaAs quantum wells under a high magnetic field (>10 T)[17]. Recently, SF was observed in $CsPbBr_3$ perovskite nanocrystals at 6 K (ref. [18]). In this Letter, we demonstrate that $MAPbI_3$ exhibits SF at higher temperatures compared to previous solid-state systems without application of a magnetic field, indicating that the versatile hybrid perovskite material system is an ideal platform to study SF and create collective coherent quantum states of matter suitable for quantum applications at elevated temperatures.

SF exhibits characteristic signatures that unambiguously help distinguish it from other collective radiation processes, such as amplified spontaneous emission (ASE). These signatures are measurable using steady-state photoluminescence (PL), time-resolved emission and time-resolved absorption spectroscopies (TASs). First, in SF, the initial population is incoherent, so there is a time delay during which spontaneous synchronization forms a macroscopic coherence[19]. Second, this delay reduces with increasing excitation density[19], and the lifetime decreases with the density N of phase-locked indistinguishable dipoles[19]. Because all the excitations interact coherently with the radiating field, the SF peak intensity scales with N^2, resulting in a quadratic excitation density dependence. Moreover, in SF, interference and propagation effects can create oscillations called Burnham–Chiao ringing in the time evolution[20]. Finally the emission kinetics of SF is similar to the relaxation of an inverted pendulum[21], leading to a specific time-dependent function based on 'sech^2', unlike the exponential behaviour of spontaneous recombination of individual excitations[22]. Here, we show that $MAPbI_3$ exhibits all of these characteristics of SF when excited above a certain threshold using ultrafast laser pulses (Supplementary Section B1).

Figure 2a shows the absorption spectra of $MAPbI_3$ at temperatures ranging from 78 K to room temperature. $MAPbI_3$ is in a tetragonal phase (TP) at room temperature and exhibits a transition to an orthorhombic phase (OP) below 150 K. The structural phase transition leads to a blueshift and a relatively sharp

[1]Department of Physics and Organic and Carbon Electronics Laboratories (ORaCEL), North Carolina State University, Raleigh, NC, USA. [2]Department of Materials Science and Engineering and Organic and Carbon Electronics Laboratories (ORaCEL), North Carolina State University, Raleigh, NC, USA. [3]These authors contributed equally: Gamze Findik, Melike Biliroglu. ✉e-mail: kgundog@ncsu.edu

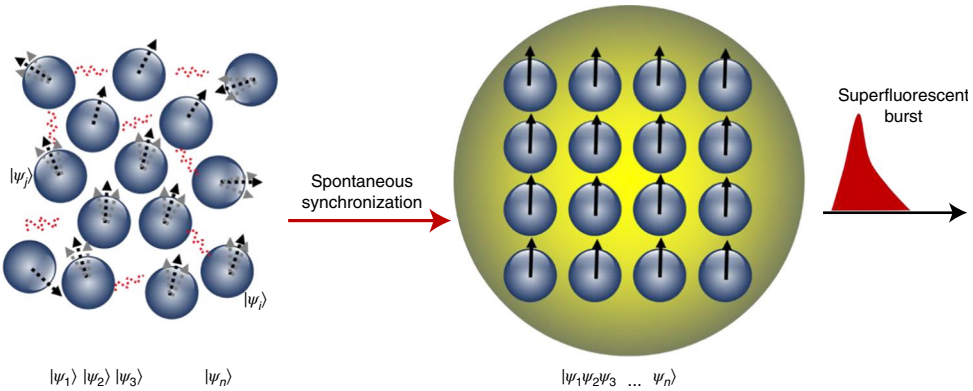

Fig. 1 | Graphic representation of SF evolution. An incoherent ensemble of dipoles is shown on the left. Arrows indicate the randomly distributed phases of individual dipoles. The red waves resemble vacuum fluctuations, which lead to spontaneous synchronization. After a time delay, the phases of the excited dipoles are locked, forming a macroscopic quantum coherent state: a 'giant atom' (on the right). This macroscopic state interacts with the radiation field collectively. The system is then described as a single wavefunction of indistinguishable particles. The collective emission of the macroscopic coherent system leads to a superfluorescent burst.

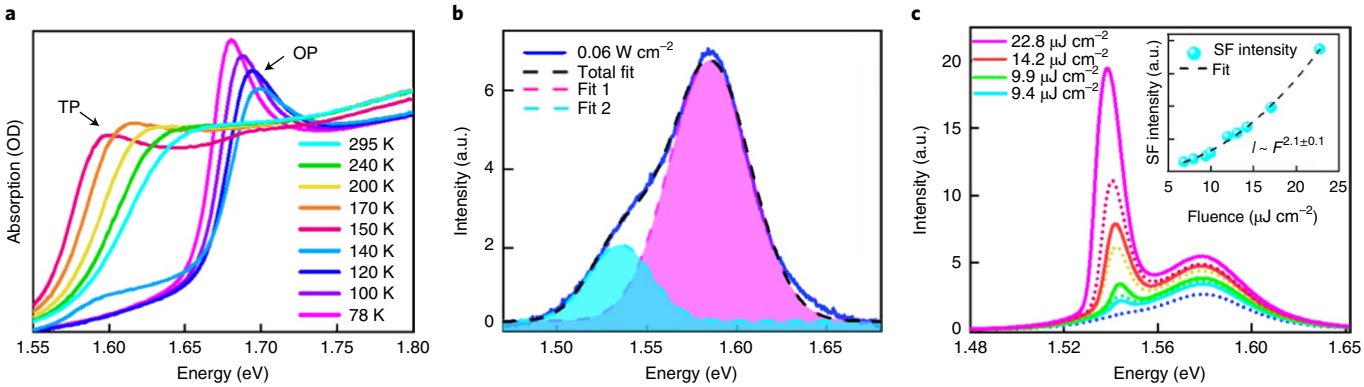

Fig. 2 | Optical measurements of $MAPbI_3$ thin films. a, Evolution of the absorption (OD: optical density) spectra of $MAPbI_3$ from 295 K to 78 K, indicating a phase transition from TP to OP below 150 K. **b**, C.w. PL measured at 78 K. Dashed lines show the two Gaussian fits for spectral features located at 1.54 eV and 1.58 eV. **c**, PL measured using pulsed excitation at different excitation fluences at 78 K. The dotted lines show the fluences for reference. The inset shows the intensity of the sharp feature extracted using Lorentzian and Gaussian fits for deconvolution. The intensity exhibits a quadratic dependence on excitation fluence with an exponent of $\alpha = 2.1 \pm 0.1$.

excitonic feature at the band edge of the absorption spectra[23]. This phase transition is incomplete, with a small fraction of TP coexisting in the OP-domain-dominant thin film[24]. Figure 2b shows the continuous-wave photoluminescence (c.w. PL) spectra at 78 K, with excitation above the OP bandgap. The c.w. PL emission has two distinct features, at 1.54 eV and at 1.58 eV, both from TP domains[23,25]. The absence of OP emission indicates the efficient transfer of excitons to the TP domains[24]. Both features increase superlinearly with the fluence, that is, $I \propto F^{1.4\pm0.1}$, indicating bimolecular recombination[26] (Supplementary Sections A1 and A2).

Figure 2c shows the PL spectra when the sample is excited with 120-fs pulses at 400 nm. The feature at 1.54 eV exhibits a threshold behaviour at ~6.3 μJ cm^{-2}. Below the threshold, both peaks increase linearly (Supplementary Fig. 7). Beyond the threshold, the 1.54-eV feature exhibits a quadratic increase up to 22.8 μJ cm^{-2}, while the 1.58-eV feature saturates. The linear increase below the threshold, as opposed to the superlinear increase at c.w. excitation ($\alpha = 1.4 \pm 0.1$), indicates excitation-density-dependent non-radiative recombination kinetics[27]. The quadratic increase of the 1.54-eV feature above the threshold indicates that the radiative recombination becomes much faster than the non-radiative processes. In the following, we show that this fast recombination process is SF.

We first characterize the time evolution of the 1.54-eV feature to investigate whether it exhibits SF dynamics. Figure 3a shows the transient PL measured at the above-threshold excitation fluences of 10.9 μJ cm^{-2} and 135.8 μJ cm^{-2} (full data are provided in Supplementary Figs. 11 and 12, temperature dependence is discussed in Supplementary Section C). The transients in Fig. 3a and Supplementary Fig. 11 have several unique characteristics of SF. First, in the range where the integrated PL increases quadratically, the peaks of the PL transients increase with fluence (F) with a power law given by $I_{max} \propto F^{3.9\pm0.7}$ (Fig. 3a, inset). This observation is consistent with SF because, in a bimolecular process, exciton density increases quadratically with fluence, so the SF peak is expected to increase with the fourth power of the fluence. Beyond 22.8 μJ cm^{-2}, as the integrated PL saturates, the peak intensity of PL transients deviates from the F^4 relationship (Supplementary Sections B2 and B3 and Supplementary Fig. 9). Next, we examine the rise and decay characteristics. At low fluence there is no measurable emission for the first 3 ps, then the PL rises slowly. However, as the excitation fluence increases, the PL signal starts earlier and rises to its peak more quickly. This density-dependent delay in PL is a signature of SF. The decay also shows faster recombination as the fluence increases (Fig. 3a), so the emission takes the shape of a burst with narrow

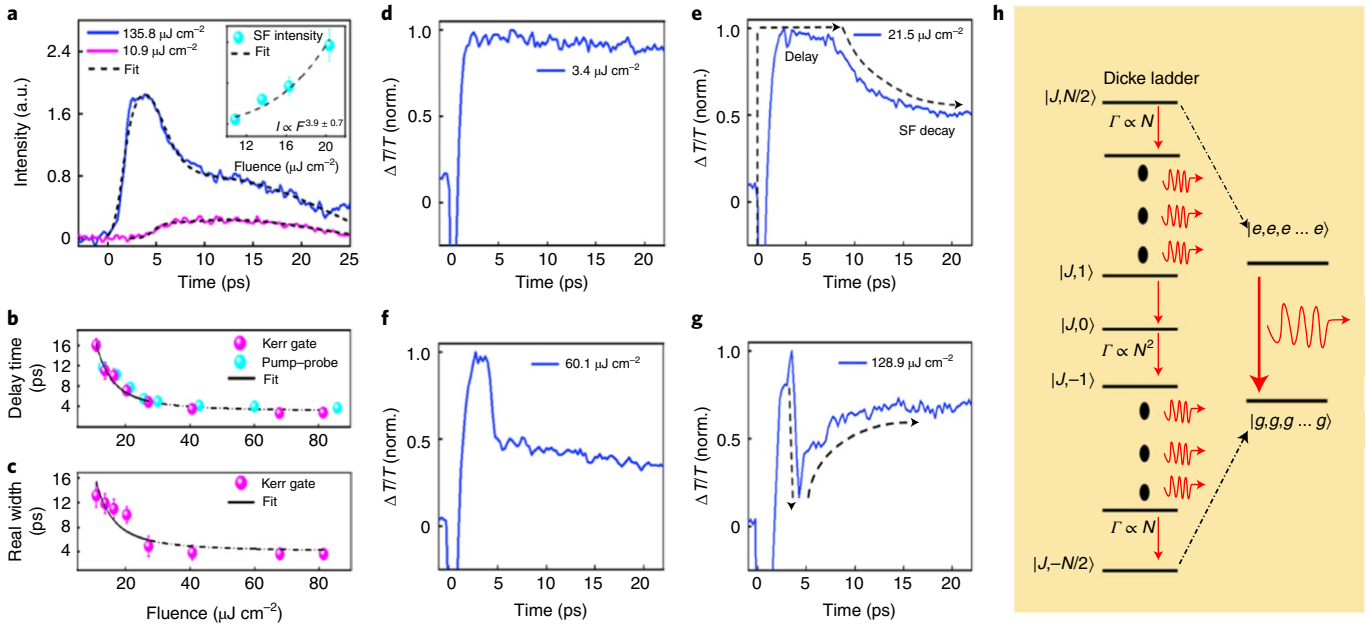

Fig. 3 | Time-resolved PL spectra and population dynamics at different excitation fluences. a, Kerr-gate PL experimental results performed at 78 K. The black dashed lines are fits to the SF model. The SF peak exhibits a clear time delay τ_D with narrowing peaks. Inset: the superlinear dependence of the SF peak intensity on excitation fluence. **b**,**c**, The extracted delay time τ_D (**b**) and real width τ_R (**c**) as a function of excitation fluence (magenta spheres). The black solid lines are fits according to the theoretical SF model. The cyan spheres are the delay time extracted from the pump–probe experiment. **d**–**g**, Population dynamics in the TP domains, measured using pump–probe experiments, probed at 1.54 eV, for excitation fluences of 3.4 μJ cm^{-2} (**d**), 21.5 μJ cm^{-2} (**e**), 60.1 μJ cm^{-2} (**f**) and 128.9 μJ cm^{-2} (**g**), respectively. Below the SF threshold (**d**), the population dynamics shows a quick capture of excitons to TP domains and a long monotonic relaxation. Above the SF threshold, the dynamics exhibits distinct intensity-dependent behaviour. The population remains steady for a period and then decays at a rate that depends on the fluence. In **e**, the horizontal dashed arrow indicates the delay time before the population starts to relax. This time period shortens with the higher excitation fluences in **f** and **g**. The decay of the coherent population is shown by the dashed arrow in **e**. With a slight increase in the excitation fluence, the decay rate increases substantially. In **g**, the SF decay rate reaches values higher than the exciton capture rate from the OP domains. As a result, SF emission depletes the population in the TP domains for a short time period. **h**, The coherent population forms a giant atom, with its relaxation path following the states in a Dicke ladder. Error bars in **a**–**c** represent 95% fit confidence intervals for the fitted data.

temporal width (real width). Although conventional exponential functions do not fit these transients, the SF theoretical models based on sech^2 functions (Supplementary equations (S5) and (S8)) fit them (black dashed lines, Fig. 3a) reasonably well[22] (Supplementary Section B4). The values of the delay time τ_D, characterizing the spontaneous synchronization period, and real width τ_R of the SF burst, obtained from these fits, are displayed as magenta spheres in Fig. 3b and 3c, respectively. Finally, as fluence increases, the emission exhibits recurrences (Supplementary Fig. 12), known as Burnham–Chiao ringing[20]. These observations, namely the fluence-dependent maximum intensity, delay time, decay and ringing behaviour, are consistent with SF.

The delay time and its density dependence are distinctive properties of SF, separating it from other collective recombination processes such as ASE[28,29]. To further investigate if the delay is due to SF, we need to show that exciton transfer from orthorhombic to tetragonal domains does not cause the fluence-dependent delayed emission. We probed population kinetics in the TP domains using TAS. Figure 3d–g shows the pump–probe traces measured at 1.54 eV at 78 K (see Supplementary Fig. 14 for all fluences). Within the first 2 ps, bandgap renormalization[30] leads to a negative signal, which quickly recovers (Supplementary Section A3). The population kinetics shows that even at the lowest fluence, the population growth in the TP domains is completed within the first 2 ps (Supplementary Fig. 5). As the excitation fluence increases beyond the threshold, the pump–probe traces show an unusual behaviour. For example, at 21.5 μJ cm^{-2}, the trace remains steady for ~8 ps, followed by an abrupt decay. Interestingly, this waiting period depends on the excitation fluence. In Fig. 3b, the cyan spheres are the waiting times measured from the pump–probe experiments and they accurately follow the τ_D values extracted from the SF model, confirming that the observed kinetics is due to SF. These observations prove that the TP population reaches its maximum within 2 ps after excitation, and the delayed PL is not due to exciton transfer, but to the macroscopic coherence buildup time.

According to SF theory, τ_D scales with $\ln N/N$, and τ_R scales as $1/N$, where N is the exciton density[19] (Supplementary Sections B4 and B5). For this analysis, one needs to determine the exciton density in the TP domains. Because the exciton formation is predominantly bimolecular, the exciton density is proportional to the square of the excited carrier density (electron–hole density n), that is, $N \propto n^2$. Using TAS, we determined the excitation fluence dependence of the TP population immediately before the SF burst was emitted. We found that, in the fluence range where the PL behaviour is quadratic, the pump–probe signal at 1.54 eV increases linearly, that is, $n \propto F$ (Supplementary Section B3). Therefore, for this range, exciton density N increases with F^2. The black solid lines in Fig. 3b,c are the $\ln N/N$ and $1/N$ curves fitting τ_D and τ_R, for the fluence range where the population increases linearly, in agreement with SF.

The population relaxation kinetics measured by the pump–probe experiment are also consistent with the SF and distinct from the dynamics expected from the ASE process. At high excitation fluences, the pump–probe signal drops rapidly (Fig. 3f,g), similar to earlier observations of SF in InGaAs quantum wells[17]. The electronic levels in the coherent macroscopic system form a Dicke ladder (Fig. 3h), where N excitations create a super-radiant

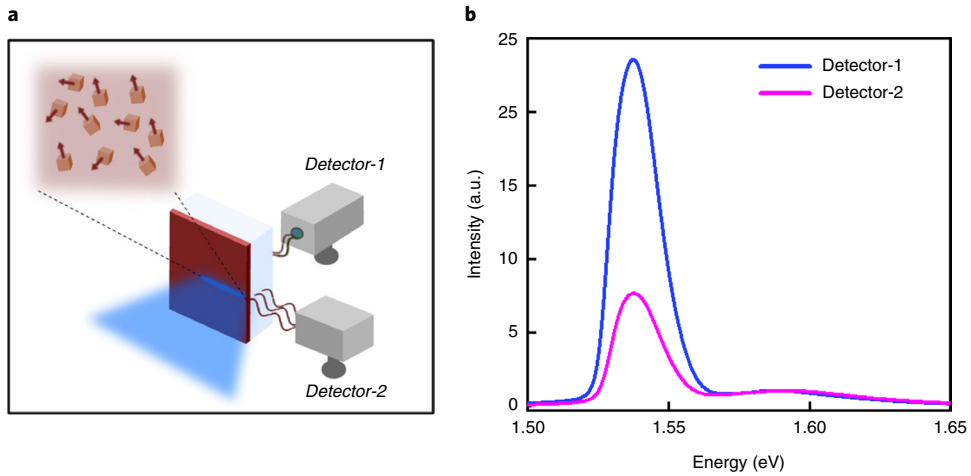

Fig. 4 | Direction-dependent PL experiment. a, Experimental schematics of direction-dependent PL measurements. PL emission is collected at two different angles at detectors 1 and 2. **b**, PL spectra collected at detectors 1 and 2, at 78 K, normalized with respect to the intensity of the 1.58-eV feature. The SF peak intensity is almost six times stronger in the forward direction (detector 1) than at the edge (detector 2). The excitation fluence is 17.4 μJ cm^{-2}.

state. The abrupt drop in the relaxation kinetics occurs because the recombination rate Γ is proportional to N at the top and bottom, and proportional to N^2 at the mid-levels of the Dicke ladder. This unique density-dependent decay rate causes a sudden population drop (Supplementary Fig. 14), which becomes as fast as 750 fs at 128.9 μJ cm^{-2} in Fig. 3g.

There is an important difference between SF and ASE: in SF, all the coherent population relaxes to the bottom of the Dicke ladder[17], which can completely deplete the population, whereas in ASE, complete depletion is impossible. In $MAPI_3$, because population depletion due to SF and refilling due to transfer from the OP domains compete, a complete depletion in the TP domains can be observed only when the SF recombination rate considerably exceeds the OP–TP exciton transfer rate. Strikingly, at the highest fluence (Fig. 3g), we observe that the sudden drop (within 750 fs) in the TP population leads to almost complete depletion and then a rise in a few picoseconds, indicating that the cooperative emission is substantially faster than the exciton capture rate from OP domains, again confirming SF.

Having established that the 1.54-eV emission is SF through analysis of the PL and population kinetics, we also studied emission directionality. In extended systems, SF exhibits strong directionality, determined with the excitation profile[31]. In $MAPbI_3$, TP domains have random sizes (100–500 nm) and shapes (Supplementary Fig. 1). If multiple TP domains establish a macroscopic coherence, then the directionality should be determined by the excitation profile. By contrast, if SF originates from individual domains, then the domain sizes and shapes should determine the SF direction. In the former, SF and ASE should have the same directionality; in the latter, SF direction becomes independent of the excitation profile and hence differs from ASE. Our studies show that SF in $MAPbI_3$ exhibits an asymmetry, with stronger forward emission than backward emission (Supplementary Section D and Supplementary Fig. 15)[32,33]. The strong forward emission is observed even when the sample is excited using a stripe-shaped beam with a spot size of 4 mm × 15 μm. In Fig. 4, the SF emission in the forward direction is stronger than the emission at the edge. Because, for a gain medium, ASE is stronger in the longer optical path direction[34], this further proves that the observed signal is not ASE, but is SF radiated from individual or small clusters of TP domains.

SF is an extremely rare phenomenon in the solid state due to the stringent requirements for macroscopic coherence[14,16,17,34]. The observation of high-temperature SF in $MAPbI_3$ suggests that hybrid perovskites are intrinsically suitable for maintaining quantum coherence. An interesting property of these materials is the strongly bound exciton polarons[35], which are known to protect coherence. For instance, in light-harvesting systems, polarons play an important role in electronic coherence and wave-like energy transfer[36]. In hybrid perovskites, polaron formation can be the reason for extended electronic coherence and the macroscopic quantum phase transition. Observation of SF in these versatile materials can make them an ideal platform for quantum applications. We anticipate that these materials can be used in various microcavities[24] as building blocks for complex systems where quantum information can be stored, processed and read out by manipulation and interrogation of giant dipoles[4,5,37,38]. Finally, from a fundamental point of view, the electronic properties of hybrid perovskites, such as the nature of the electronic states, their localization, coupling to phonons modes and dephasing kinetics, have to be further studied to fully understand the dynamics leading to SF.

Online content

Any methods, additional references, Nature Research reporting summaries, source data, extended data, supplementary information, acknowledgements, peer review information; details of author contributions and competing interests; and statements of data and code availability are available at https://doi.org/10.1038/s41566-021-00830-x.

Received: 24 November 2020; Accepted: 12 May 2021;
Published online: 21 June 2021

References

1. Torchinsky, D. H., Mahmood, F., Bollinger, A. T., Božović, I. & Gedik, N. Fluctuating charge-density waves in a cuprate superconductor. *Nat. Mater.* **12**, 387–391 (2013).
2. Li, T. et al. Femtosecond switching of magnetism via strongly correlated spin–charge quantum excitations. *Nature* **496**, 69–73 (2013).
3. Keeling, J., Marchetti, F., Szymańska, M. & Littlewood, P. Collective coherence in planar semiconductor microcavities. *Semicond. Sci. Technol.* **22**, R1–R26 (2007).
4. Bergmann, M. & Gühne, O. Entanglement criteria for Dicke states. *J. Phys. A* **46**, 385304 (2013).
5. Tóth, G. & Apellaniz, I. Quantum metrology from a quantum information science perspective. *J. Phys. A* **47**, 424006 (2014).

6. Whitfield, J. Synchronized swinging. *Nature* https://doi.org/10.1038/news020218-16 (2002).
7. Eastham, P. R. & Rosenow, B. in *Universal Themes of Bose–Einstein Condensation* (eds Proukakis, N. P. et al.) 462–476 (Cambridge Univ. Press, 2017).
8. Dicke, R. H. Coherence in spontaneous radiation processes. *Phys. Rev.* **93**, 99–110 (1954).
9. Li, X. et al. Observation of Dicke cooperativity in magnetic interactions. *Science* **361**, 794–797 (2018).
10. Scully, M. O. & Svidzinsky, A. A. The super of superradiance. *Science* **325**, 1510–1511 (2009).
11. Thompson, J. V. et al. Pulsed cooperative backward emissions from non-degenerate atomic transitions in sodium. *New J. Phys.* **16**, 103017 (2014).
12. Skribanowitz, N., Herman, I. P., MacGillivray, J. C. & Feld, M. S. Observation of Dicke superradiance in optically pumped HF gas. *Phys. Rev. Lett.* **30**, 309–312 (1973).
13. Ariunbold, G. O. et al. Observation of picosecond superfluorescent pulses in rubidium atomic vapor pumped by 100-fs laser pulses. *Phys. Rev. A* **82**, 043421 (2010).
14. Florian, R., Schwan, L. O. & Schmid, D. Two-color superfluorescence of O_2^- centers in KCl. *J. Lumin.* **31**, 169–171 (1984).
15. Miyajima, K., Kumagai, Y. & Ishikawa, A. Ultrashort radiation of biexcitonic superfluorescence from high-density assembly of semiconductor quantum dots. *J. Phys. Chem. C* **121**, 27751–27757 (2017).
16. Dai, D. & Monkman, A. Observation of superfluorescence from a quantum ensemble of coherent excitons in a ZnTe crystal: evidence for spontaneous Bose–Einstein condensation of excitons. *Phys. Rev. B* **84**, 115206 (2011).
17. Noe, G. T. II et al. Giant superfluorescent bursts from a semiconductor magneto-plasma. *Nat. Phys.* **8**, 219–224 (2012).
18. Rainò, G. et al. Superfluorescence from lead halide perovskite quantum dot superlattices. *Nature* **563**, 671–675 (2018).
19. Benedict, M. G. *Super-Radiance*: *Multiatomic Coherent Emission* (CRC Press, 1996).
20. Burnham, D. C. & Chiao, R. Y. Coherent resonance fluorescence excited by short light pulses. *Phys. Rev.* **188**, 667–675 (1969).
21. Gross, M. & Haroche, S. Superradiance: an essay on the theory of collective spontaneous emission. *Phys. Rep.* **93**, 301–396 (1982).
22. Bonifacio, R. & Lugiato, L. Cooperative radiation processes in two-level systems: superfluorescence. *Phys. Rev. A* **11**, 1507–1521 (1975).
23. Osherov, A. et al. The impact of phase retention on the structural and optoelectronic properties of metal halide perovskites. *Adv. Mater.* **28**, 10757–10763 (2016).
24. Jia, Y., Kerner, R. A., Grede, A. J., Rand, B. P. & Giebink, N. C. Continuous-wave lasing in an organic–inorganic lead halide perovskite semiconductor. *Nat. Photon.* **11**, 784–788 (2017).
25. Chuliá-Jordán, R. et al. Inhibition of light emission from the metastable tetragonal phase at low temperatures in island-like films of lead iodide perovskites. *Nanoscale* **11**, 22378–22386 (2019).
26. Phuong, L. Q. et al. Free carriers versus excitons in $CH_3NH_3PbI_3$ perovskite thin films at low temperatures: charge transfer from the orthorhombic phase to the tetragonal phase. *J. Phys. Chem. Lett.* **7**, 2316–2321 (2016).
27. Milot, R. L., Eperon, G. E., Snaith, H. J., Johnston, M. B. & Herz, L. M. Temperature-dependent charge-carrier dynamics in $CH_3NH_3PbI_3$ perovskite thin films. *Adv. Funct. Mater.* **25**, 6218–6227 (2015).
28. Malcuit, M. S., Maki, J. J., Simkin, D. J. & Boyd, R. W. Transition from superfluorescence to amplified spontaneous emission. *Phys. Rev. Lett.* **59**, 1189–1192 (1987).
29. Siegman, A. E. *Lasers* (University Science Books, 1986).
30. Miyata, K. et al. Large polarons in lead halide perovskites. *Sci. Adv.* **3**, e1701217 (2017).
31. Jho, Y. et al. Cooperative recombination of a quantized high-density electron–hole plasma in semiconductor quantum wells. *Phys. Rev. Lett.* **96**, 237401 (2006).
32. Ariunbold, G. O., Sautenkov, V. A., Rostovtsev, Y. V. & Scully, M. O. Ultrafast laser control of backward superfluorescence towards standoff sensing. *Appl. Phys. Lett.* **104**, 021114 (2014).
33. Kuan, Y.-H. & Liao, W.-T. Transition between amplified spontaneous emission and superfluorescence in a longitudinally pumped medium by an X-ray free-electron-laser pulse. *Phys. Rev. A* **101**, 023836 (2020).
34. Vardeny, Z. V. *Ultrafast Dynamics and Laser Action of Organic Semiconductors* (CRC Press, 2009).
35. Thouin, F. et al. Phonon coherences reveal the polaronic character of excitons in two-dimensional lead halide perovskites. *Nat. Mater.* **18**, 349–356 (2019).
36. Ishizaki, A. & Fleming, G. R. Theoretical examination of quantum coherence in a photosynthetic system at physiological temperature. *Proc. Natl Acad. Sci. USA* **106**, 17255–17260 (2009).
37. Wang, Z. et al. Controllable switching between superradiant and subradiant states in a 10-qubit superconducting circuit. *Phys. Rev. Lett.* **124**, 013601 (2020).
38. Ariunbold, G. O., Sautenkov, V. A. & Scully, M. O. Temporal coherent control of superfluorescent pulses. *Opt. Lett.* **37**, 2400–2402 (2012).

Methods

Synthesis of $MAPbI_3$ thin films. Lead iodide (99.999%), dimethylformamide (anhydrous, 99.8%), dimethyl sulfoxide (anhydrous, 99.9%) and toluene (anhydrous, 99.8%) were purchased from Sigma-Aldrich. Methyl ammonium iodide was purchased from Dyesol. The perovskite precursor solution was prepared by dissolving PbI_2, MAI and dimethyl sulfoxide (DMSO) (molar ratio of 1:1:1) in dimethylformamide (DMF) at a concentration of 1 M. The precursor solution was spin-coated on a glass substrate, during which 100 µl of toluene was dropped on the sample at the eighth second. The precursor film was then annealed at 100 °C for 10 min to complete the crystallization.

Structure characterization. The samples used in this work are 300 nm thick. A scanning electron microscopy image is shown in Supplementary Fig. 1a (where the diagonal line is 5.18 µm long). The average grain size is ~260 nm. Supplementary Fig. 1b shows an atomic force microscopy image. The surface roughness (root mean square) is 10.6 nm. In addition, room-temperature X-ray diffraction data show the signature (110) peak around 14.8° for the $MAPbI_3$ perovskite-type tetragonal lattice. The other peaks suggest the film is not textured, meaning there is no preferred orientation.

PL experiments. A Mightex spectrometer was used to measure the PL. The sample was excited using 400-nm pulses obtained by frequency doubling of the output of a Ti:sapphire amplifier with a repetition rate of 1 kHz and with the central frequency at 800 nm. For the c.w. experiments, a 445-nm InGaN laser was used to excite the sample.

Kerr-gate experiment. Time-resolved SF was measured with a home-built Kerr-gate set-up using a 1-kHz amplified Ti:sapphire laser (Quantronix Integra-C) with 120-fs pulsed output at 800 nm. As shown in Supplementary Fig. 2, the laser output beam was split into two paths, one for the optical Kerr-gate pulse and the other for the excitation beam, which was converted to 400 nm through second harmonic generation using a beta barium borate crystal. The collected PL and the gate pulse were focused on CS_2 in a 2-mm-thick cuvette, which was used as the Kerr medium. The gated signal was measured with a Hamamatsu photomultiplier tube (H10721-20) attached to a monochromator. The sample was kept in a Janis continuous-flow liquid-nitrogen cryostat. The excitation beam size was 1.5 mm.

Time-resolved pump–probe experiment. The pump–probe measurements were performed in a commercial Helios system. The excitation source was an amplified Ti:sapphire laser (Coherent Libra) system producing 100-fs pulses at 800 nm and with a 1-kHz repetition rate. For the pump path, we frequency doubled the 800-nm pulses. Probe pulses were produced by white-light continuum generation in a sapphire crystal.

Time-correlated single-photon counting. We used a home-built time-correlated single-photon-counting set-up with 300-ps time resolution for measuring the long-time PL kinetics. In the experiment, the output of a Ti:sapphire amplifier was frequency doubled using a beta barium borate crystal. The PL was collected and guided into a monochromator and detected with a Hamamatsu PMT system (H10721-20).

Data availability

Data that support the plots within this paper and other findings of this study are available from the corresponding author upon reasonable request. Source data are provided with this paper.

Acknowledgements

We acknowledge helpful discussions with J. Thomas (NC State University), D. Aspnes (NC State University) and V. Temnov (IMMM Le Mans). We also acknowledge support from the NCSU Imaging and Kinetic Spectroscopy facility and technical support from E. Danilov for the time-resolved absorption experiment. K.G. and F.S. acknowledge support from the National Science Foundation Designing Materials to Revolutionize and Engineer our Future programme (grant 1729383) and the NC State University Research and Innovation Seed Funding (RISF).

Author contributions

G.F. and M.B. performed the PL and TRPL measurements and pump–probe experiments and analysed the results. D.S. assisted with the pump–probe experiments and H.A. provided help with TRPL experiments. A.B. performed steady-state absorption and PL experiments. L.L., Q.D. and F.S. provided the samples. K.G. conceived the research problems and coordinated the studies. K.G. drafted the manuscript with the help of G.F. and M.B. All authors helped with editing the manuscript.

Competing interests

The authors declare no competing interests.

Additional information

Supplementary information The online version contains supplementary material available at https://doi.org/10.1038/s41566-021-00830-x.

Correspondence and requests for materials should be addressed to K.G.

Peer review information *Nature Photonics* thanks Gombojav Ariunbold and the other, anonymous, reviewer(s) for their contribution to the peer review of this work.

Reprints and permissions information is available at www.nature.com/reprints.